

Electronic Structure of Atoms, Molecules and Solids from (e,2e) Studies*

I. E. McCarthy

Electronic Structure of Materials Centre, Flinders University of South Australia, Bedford Park, S.A. 5042, Australia.

Abstract

The (e,2e) reaction on atoms can be described quite well in most of kinematic space by distorted-wave theories of varying sophistication. In some regions it is necessary to obey the newly-discovered boundary condition for three charged particles. The understanding enables us to recognise a kinematic region where the reaction is sensitive only to the target-ion structure. Single-particle and electron-correlation information has been discovered for a wide range of atoms and molecules. The understanding of solids is developing.

1. Introduction

Electronic structure is directly observed by kinematically-complete ionisation experiments (McCarthy and Weigold 1988). Relevant observed quantities are defined by Fig. 1. We adopt the convention that the momentum of the faster outgoing electron is labelled by \mathbf{k}_A .

The experiment observes several quantities of theoretical significance. The electron separation energy ϵ_f is defined by

$$\epsilon_f = E_0 - E_A - E_B. \quad (1)$$

It is the difference between the ground-state energy of the target and the energy of the eigenstate f of the ion. The experiment observes the energy spectrum of the ion.

The recoil momentum of the ion in the state f is observed. It is

$$\mathbf{p} = \mathbf{k}_0 - \mathbf{k}_A - \mathbf{k}_B = -\mathbf{q}. \quad (2)$$

The most naive interpretation of the experiment is the plane-wave impulse approximation (PWIA). Here the electron is cleanly knocked out of the target so that the recoil momentum \mathbf{p} is equal and opposite to the momentum \mathbf{q} of the electron in the target at the reaction instant. If the target structure is interpreted by the most naive structure model, the one-electron model, the distribution of the differential cross section for the reaction against \mathbf{p} is

* Paper presented at the Workshop on Interfaces in Molecular, Electron and Surface Physics, held at Fremantle, Australia, 4-7 February 1990.

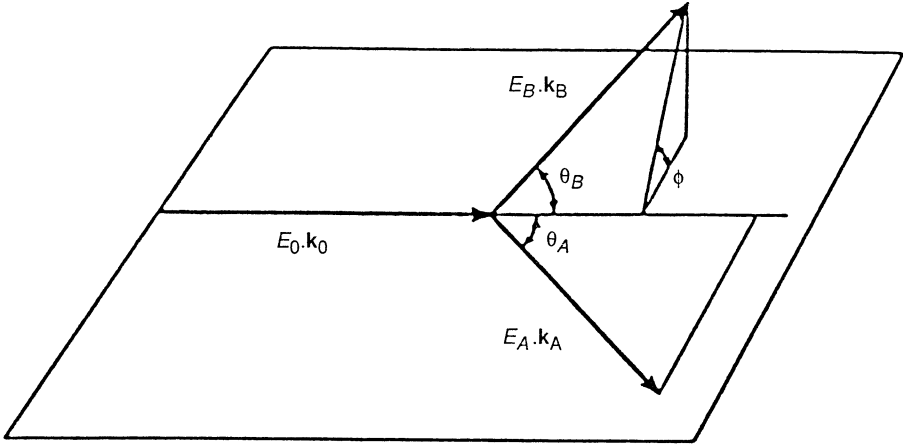


Fig. 1. Definition of the kinematic quantities in the (e, 2e) reaction.

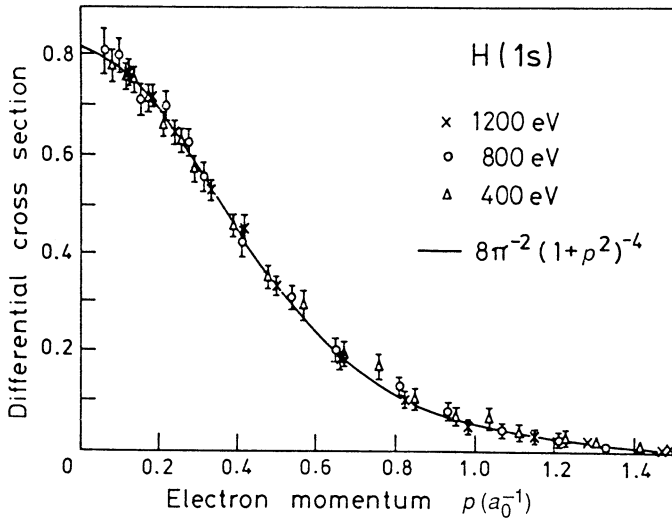


Fig. 2. Distribution of the recoil momentum in the noncoplanar symmetric (e, 2e) reaction on atomic hydrogen at different total energies (Lohmann and Weigold 1981).

proportional to the square of the one-electron orbital for the one-hole state i . In most experiments the target is not aligned. Therefore we observe only the spherically-averaged distribution of electron momentum against p .

A quantity of interest in considering the range of validity of approximations is the momentum transfer \mathbf{K} from the incident electron to the faster electron

$$\mathbf{K} = \mathbf{k}_0 - \mathbf{k}_A. \quad (3)$$

In this paper I discuss the type of structure information that can be obtained from (e, 2e) and the range of validity of different theoretical interpretations of the reaction, particularly the PWIA.

For orientation we first consider the (e, 2e) reaction on atomic hydrogen, whose electron momentum distribution we know to be proportional to $(1+q^2)^{-4}$. The experimental kinematics most commonly used for structure applications is the noncoplanar symmetric kinematics, in which $E_A = E_B$, $\theta_A = \theta_B$ and ϕ is varied. The simplest interpretation of the reaction expects the cross section to be proportional to the momentum distribution of the struck electron and also to K^{-4} , which is the Rutherford cross section for two electrons. Since K is independent of θ in noncoplanar symmetric kinematics, we expect the cross section as a function of p to be strictly proportional to the electron momentum distribution. Fig. 2 shows that this is so at total energy ($E_A + E_B$) of 400, 800 and 1200 eV. Not only must the PWIA be taken seriously as a good first approximation, but the apparent structure information is identified as true structure information since it is independent of the probe conditions, in this case the total energy.

2. Simple Theory of Ionisation

We first discuss the plane-wave impulse approximation, which corresponds not only to our naive intuition, but to the results of an actual experiment for hydrogen. The approximation represents initial and final states as antisymmetrised products of free-electron wave functions (plane waves) and eigenstates of the target and ion respectively. Since the electrons are approximated to interact only with each other at the collision instant we represent this interaction by its full amplitude t_S for spin state S . The (e,2e) amplitude is

$$T_f(\mathbf{k}_0, \mathbf{k}_A, \mathbf{k}_B) = \langle \mathbf{k}_A \mathbf{k}_B f | t_S | 0 \mathbf{k}_0 \rangle. \quad (4)$$

The corresponding differential cross section is

$$\frac{d^5 \sigma_f}{d\Omega_A d\Omega_B dE_A} = (2\pi)^4 \frac{k_A k_B}{k_0} (4\pi)^{-1} \int d\hat{\mathbf{p}} \sum_{av} |T_f(\mathbf{k}_0, \mathbf{k}_A, \mathbf{k}_B)|^2, \quad (5)$$

where \sum_{av} indicates a sum over final-state degeneracies and average over initial-state degeneracies.

Making the transformation from particle momenta to relative and centre-of-mass momenta in the (linear) exponents of the plane waves in (4) we rewrite (4) as

$$T_f(\mathbf{k}_0, \mathbf{k}_A, \mathbf{k}_B) = \langle \mathbf{k}' | t_S(k'^2) | \mathbf{k} \rangle \langle f | 0 \mathbf{p} \rangle. \quad (6)$$

In this approximation the amplitude factorises into an ee collision amplitude and the structure overlap, which is the overlap of the ion wave function with a wave function representing a hole of momentum \mathbf{p} in the target, sometimes called the Dyson amplitude.

The ee collision amplitude is the antisymmetrised half-off-shell t -matrix element for total spin S , representing the solution of the equal-mass Coulomb scattering problem for relative kinetic energy k'^2 and the corresponding final relative momentum

$$\mathbf{k}' = \frac{1}{2}(\mathbf{k}_A - \mathbf{k}_B). \quad (7)$$

The initial relative momentum in this amplitude,

$$\mathbf{k} = \frac{1}{2}(\mathbf{k}_0 + \mathbf{p}), \quad (8)$$

does not correspond to the relative kinetic energy. Hence the amplitude is said to be half off shell.

All kinematic quantities in (5) and (6) are observed in the experiment and the ee collision amplitude is known (Ford 1964). Hence we have a theory for the differential cross section, given the structure overlap. In other words the reaction directly observes the structure overlap, or more strictly according to (5), its absolute square, spherically averaged and summed over degeneracies.

For all targets the degeneracies include the spin degeneracy of the ee collision and the magnetic degeneracies of the electronic states. For molecules we do not resolve vibrational or rotational states so these are effectively degeneracies, which are summed out by closure relations (McCarthy and Weigold 1988), assuming that their degrees of freedom are independent of the electronic degrees of freedom. The structure overlap therefore is effectively the electronic structure overlap.

3. Structure Determination

We now take a closer look at the electronic structure overlap. The simplest approximation, which orients our understanding, is the one-electron approximation. The best one-electron approximation represents the target by a determinant of variationally-determined (Hartree-Fock) one-electron orbitals and the ion by one hole for the orbital i in this determinant. If we are tempted to consider whether the ion Hartree-Fock orbitals may give a better approximation we should consider hydrogen! In this approximation the ion state $|f\rangle$ is identical to the one-hole state $|i\rangle$. The structure overlap is the momentum-space orbital $\psi_i(\mathbf{p})$.

It is appropriate now to consider the first (e,2e) experiment to observe valence structure, the 400 eV noncoplanar symmetric experiment on argon by Weigold *et al.* (1973). Fig. 3 shows the distribution of separation energies. We notice that there are more ion states than the two we expect from holes in the valence orbitals 3p and 3s, whose Hartree-Fock energies are 16 and 35 eV respectively. How do we understand these states?

We have a new tool at our disposal, the momentum distribution. Fig. 4 shows the momentum distribution for the state at 16 eV compared with three PWIA calculations. The 3p Hartree-Fock orbital describes the data exactly. Two other quite sensible orbitals, Hartree-Fock-Slater and a variationally-optimised hydrogenic 3p function, are noticeably worse. Not only does our simplest description work perfectly for this state but the orbital is determined very sensitively.

What about the state at 29 eV and several unresolved higher states? Fig. 5 shows their momentum distributions, observed with better resolution in a later experiment (Weigold and McCarthy 1978). The PWIA with the Hartree-Fock 3s orbital works well for all of them for $p < 1$ a.u. Its cross section is rather too small for higher p , but the states are certainly associated with the 3s orbital. What is this relationship?

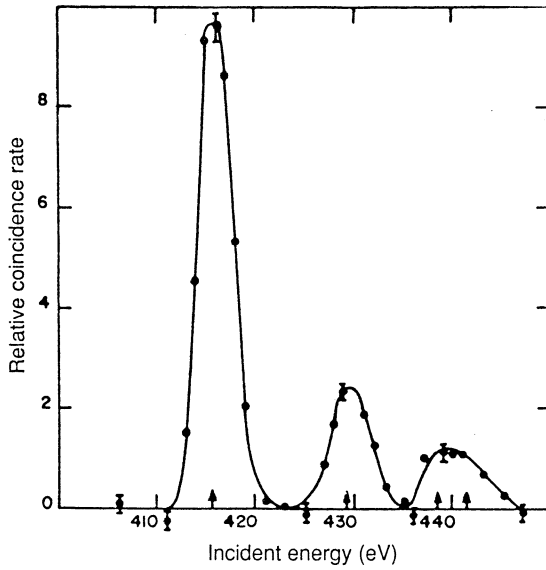


Fig. 3. Differential cross section at $\phi = 10^\circ$ for the 400 eV noncoplanar symmetric (e, 2e) reaction on argon (Weigold *et al.* 1973). The arrows indicate known energy levels of Ar.

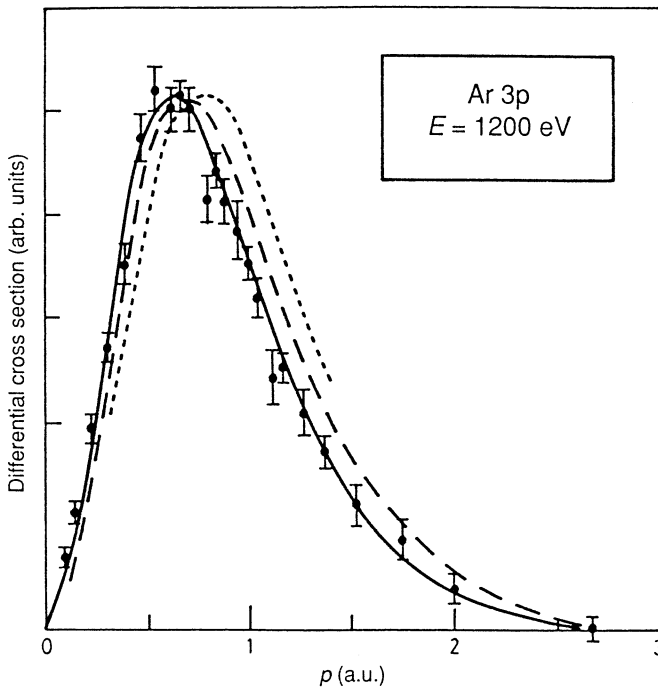


Fig. 4. The 1200 eV noncoplanar symmetric momentum distribution for the 15.76 eV state of Ar (McCarthy and Weigold 1988). Curves are PWIA calculated with 3p orbitals: Full, Hartree-Fock; long-dashed, Hartree-Fock-Slater; short-dashed, hydrogenic (variational).

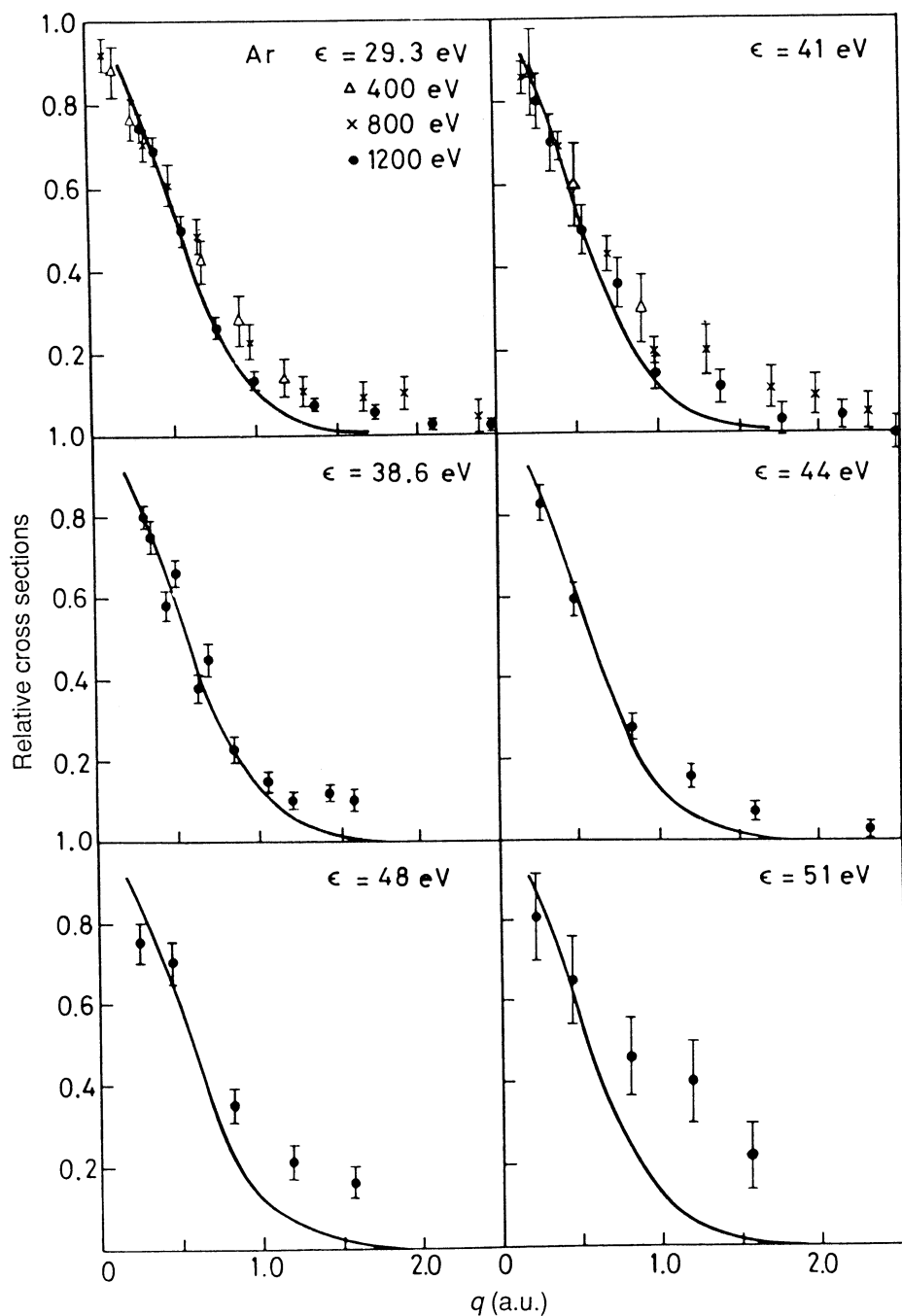


Fig. 5. The noncoplanar symmetric momentum distribution for excited states of Ar (Weigold and McCarthy 1978) at different total energies. Curves are PWIA calculated with 3s Hartree-Fock orbitals.

To understand the structure overlap we consider the configuration-interaction (CI) expansion of target and ion states in determinants (configurations) formed by occupying target Hartree-Fock orbitals by electrons in such a way that each configuration has the symmetry of the state. The configuration with all the lowest orbitals occupied is the Hartree-Fock configuration. The representation we want to consider for the ion is not the CI representation, but one in which the orthonormal basis states $|j\rangle$ are linear combinations of configurations formed by putting one hole in a target eigenstate. This is the weak-coupling representation and the basis states $|j\rangle$ are weak-coupling states. Note that the weak-coupling states are identical to the CI configurations if the target is uncorrelated, i.e. represented by the Hartree-Fock configuration

$$\langle f | 0\mathbf{p} \rangle = \sum_j \langle f | j \rangle \langle j | 0\mathbf{p} \rangle. \quad (9)$$

Clearly $\langle j | 0\mathbf{p} \rangle$ is zero if $|j\rangle$ is not a one-hole state $|i\rangle$ formed by putting a hole in the target ground state.

The weak-coupling approximation has turned out to be usually valid. Here the weak-coupling expansion of the ion state $|f\rangle$ contains only a single one-hole state $|i\rangle$

$$\langle f | 0\mathbf{p} \rangle = \langle f | i \rangle \langle i | 0\mathbf{p} \rangle. \quad (10)$$

The cross section in this approximation is proportional to the square of the one-hole overlap $|\langle i | 0\mathbf{p} \rangle|^2$, which is very close to the square of the momentum-space orbital $|\psi_i(\mathbf{p})|^2$. It is proportional also to the spectroscopic factor $|\langle f | i \rangle|^2$, which is the probability of finding the one-hole state $|i\rangle$ in the weak-coupling expansion of the ion state $|f\rangle$.

Ion states that do not obey the weak-coupling approximation are of special interest in studying target correlations. The simplest example is helium, considered as a linear combination of $1s1s$ and $1s2s$ configurations. The $2s$ ion state is not a one-hole state. Its overlap with the target state is proportional to the coefficient of $1s2s$, thus giving information about the $1s2s$ configuration that is not swamped by the large contribution from $1s1s$.

The example of the $3s$ hole in argon is one that can be treated in the weak-coupling approximation. There is a manifold of ion states, each containing the $3s$ -hole state. We call it the $3s$ manifold. Consider the sum of cross sections for all the ion states $|f\rangle$ belonging to the i manifold. According to (10) and the fact that $|i\rangle$ is normalised, the sum is proportional to

$$\sum_f |\langle f | 0\mathbf{p} \rangle|^2 = \sum_f \langle \mathbf{p}0 | i \rangle \langle i | f \rangle \langle f | i \rangle \langle i | 0\mathbf{p} \rangle = |\langle i | 0\mathbf{p} \rangle|^2. \quad (11)$$

The sum is therefore the cross section for the one-hole overlap, or essentially for the orbital $\psi_i(\mathbf{p})$. This gives an experimental definition of an orbital.

The energy ϵ_i for the one-hole configuration $|i\rangle$, the orbital energy, is defined to be the expectation value of the ion Hamiltonian H for the configuration $|i\rangle$:

$$\epsilon_i = \langle i | H | i \rangle = \sum_f \langle i | H | f \rangle \langle f | i \rangle = \sum_f |\langle f | i \rangle|^2 \epsilon_f. \quad (12)$$

The orbital energy is thus the centroid of the energies of the i manifold, weighted by the spectroscopic factors. In the case of the $3s$ manifold of argon this is at 35 eV, agreeing with the $3s$ Hartree-Fock energy.

There are now two loose ends to be tied up in our interpretation of the argon experiments. First the 3s orbital does not describe the shape of the 3s momentum distribution exactly. It is too small for large p . Second we have not yet checked whether normalised 3p and 3s orbitals describe the relationship between the cross sections for the whole 3p and 3s manifolds. For this we need some more theory.

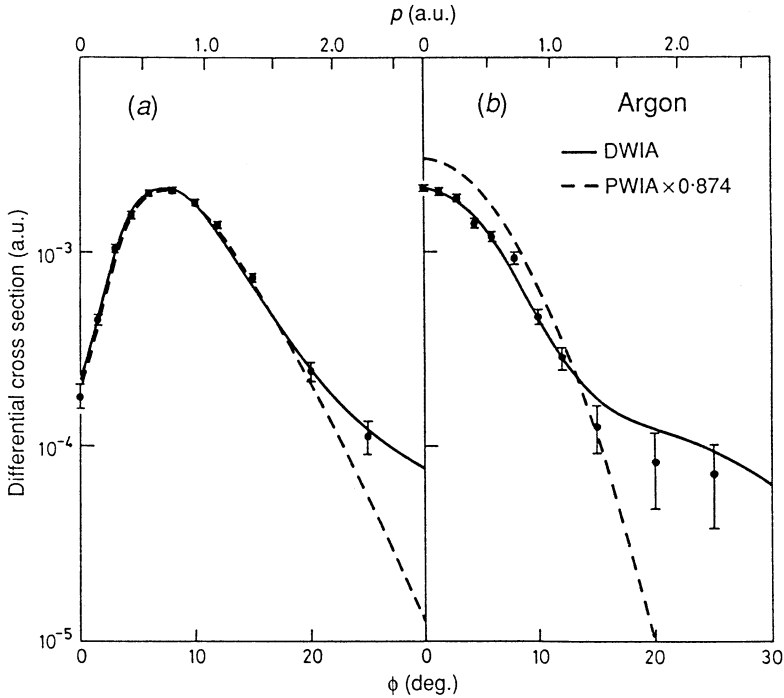


Fig. 6. The 1500 eV noncoplanar symmetric momentum distributions for the (a) 3p and (b) 3s manifolds of argon (McCarthy *et al.* 1989). The experiment is normalised to the 3p peak.

4. Distorted-wave Theories

The distorted-wave impulse approximation (DWIA) replaces the plane waves in the structure overlap of (6) by wave functions describing the scattering of electrons in the spherically-averaged static potentials of the target and ion in the initial and final states respectively:

$$T_f(\mathbf{k}_0, \mathbf{k}_A, \mathbf{k}_B) = \langle \mathbf{k}' | t_S(k'^2) | \mathbf{k} \rangle \langle \chi^{(-)}(\mathbf{k}_A) \chi^{(-)}(\mathbf{k}_B) f | 0 \chi^{(+)}(\mathbf{k}_0) \rangle. \tag{13}$$

This approximation is based on the intuition we have obtained by the iterative interaction between theory and experiment. Fig. 6 shows how it works for the 3s and 3p manifolds of argon (McCarthy *et al.* 1989) at 1500 eV, using the weak-coupling approximation (10). The noncoplanar symmetric experimental data are normalised to the calculation at one point, the peak of the 3p DWIA curve. Both our loose ends are tied up. The relationship between 3p and 3s manifolds is described perfectly by DWIA, but not by PWIA. The large- p cross

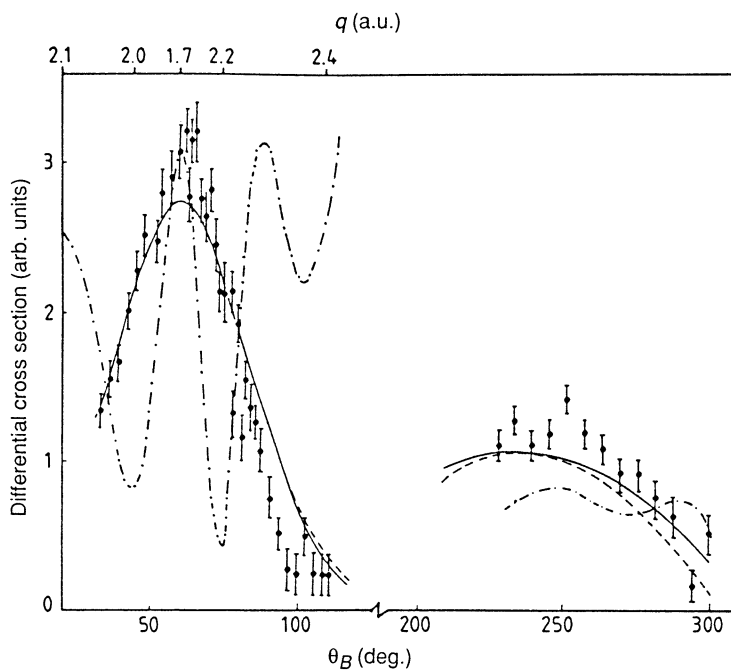


Fig. 7. Differential cross section for the coplanar asymmetric (e, 2e) reaction on the 3p orbital of argon (Avaldi *et al.* 1989a): $E_A = 880$ eV, $\theta_A = 8^\circ$, $E_B = 120$ eV. Curves are full, PWIA with a 15 eV energy shift; broken, PWIA; dot-dash, DWIA.

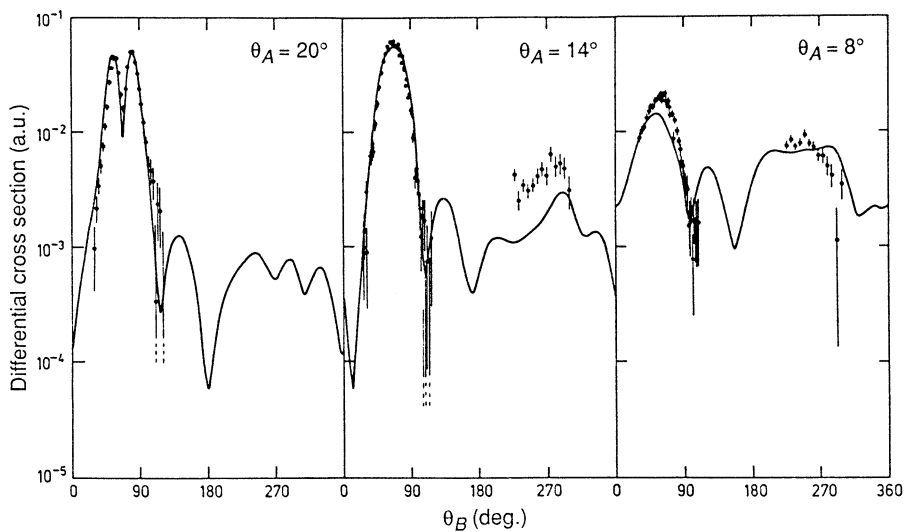


Fig. 8. Differential cross section for the coplanar asymmetric (e, 2e) reaction on the 3p orbital of argon (Avaldi *et al.* 1989b): $E_A = 880$ eV, $E_B = 120$ eV. Curves are DWBA.

sections are described perfectly by DWIA, but the discrepancy observed for the PWIA in Fig. 5 is made more explicit in the more-accurate experiment. The noncoplanar symmetric argon experiment is thus completely understood by using the DWIA for the reaction and the weak-coupling approximation for the target-ion structure.

At this stage it is important to point out that the success of the DWIA for the noncoplanar symmetric (e, 2e) reaction is not repeated in other kinematic arrangements. Fig. 7 shows an experiment (Avaldi *et al.* 1989a) on the 3p state of argon in which $E_A = 880$ eV, $E_B = 120$ eV, $\theta_A = 8^\circ$. In this experiment p is always much greater than 1 a.u. The DWIA (dot-dash curve) is a complete failure, even compared to the PWIA (solid curve). It turns out (Madison *et al.* 1989) that this is due to the invalidity of the factorisation involved in going from (4) to (6) with distorted waves. The factorisation is exact for plane waves. It is impossible to calculate the unfactorised form obtained by introducing the distorted waves in (4).

We can calculate the distorted-wave Born approximation (DWBA) obtained by approximating t_S in (4) by its first-order form v_S (the ee potential with exchange) and introducing distorted waves:

$$T_f(\mathbf{k}_0, \mathbf{k}_A, \mathbf{k}_B) = \langle \chi^{(-)}(\mathbf{k}_A) \chi^{(-)}(\mathbf{k}_B) f | v_S | 0 \chi^{(+)}(\mathbf{k}_0) \rangle. \quad (14)$$

This approximation describes the large cross sections for the asymmetric (e, 2e) reaction on the 3p state of argon much better (Avaldi *et al.* 1989b), particularly for $\theta_A = 20^\circ$ and 14° , where p is less than 1 a.u. This is shown in Fig. 8.

It is interesting to consider what is the best possible description of the (e, 2e) reaction. Here we start from the formally-correct T -matrix element, considering hydrogen as the simplest target:

$$T(\mathbf{k}_0, \mathbf{k}_A, \mathbf{k}_B) = \langle \Phi^{(-)}(\mathbf{k}_A, \mathbf{k}_B) | V_S | \Psi_0^{(+)}(\mathbf{k}_0) \rangle \quad (15)$$

$$= \langle \Psi^{(-)}(\mathbf{k}_A, \mathbf{k}_B) | V_S | 0 \mathbf{k}_0 \rangle. \quad (16)$$

Here Ψ indicates a complete three-body wave function and $\Phi^{(-)}$ indicates the asymptotic wave function for three outgoing charged particles. Until 1989 $\Phi^{(-)}$ was not fully established. Brauner *et al.* (1989) showed that it is two plane waves multiplied by three Coulomb phase factors, one for each pair of particles. They used an approximation for $\Psi^{(-)}$ in (16) which is two distorted waves calculated in the ion potential and the Coulomb factor for the relative ee motion. This approximation is illustrated for coplanar asymmetric experiments in Fig. 9, together with the DWBA (14) and an approximation to (15) due to Curran and Walters (1987) who use the same final state as the DWBA, but represent $\Psi_0^{(+)}(\mathbf{k}_0)$ by a wave function taken from a detailed scattering calculation in which the first three states of hydrogen are represented exactly and the remainder (including the continuum) are represented by pseudostates with parameters fitted to approximate scattering calculations. The three-body wave function of Brauner *et al.* is clearly the best approximation. The DWBA is again quite good for the large cross sections, but tends to overestimate magnitudes.

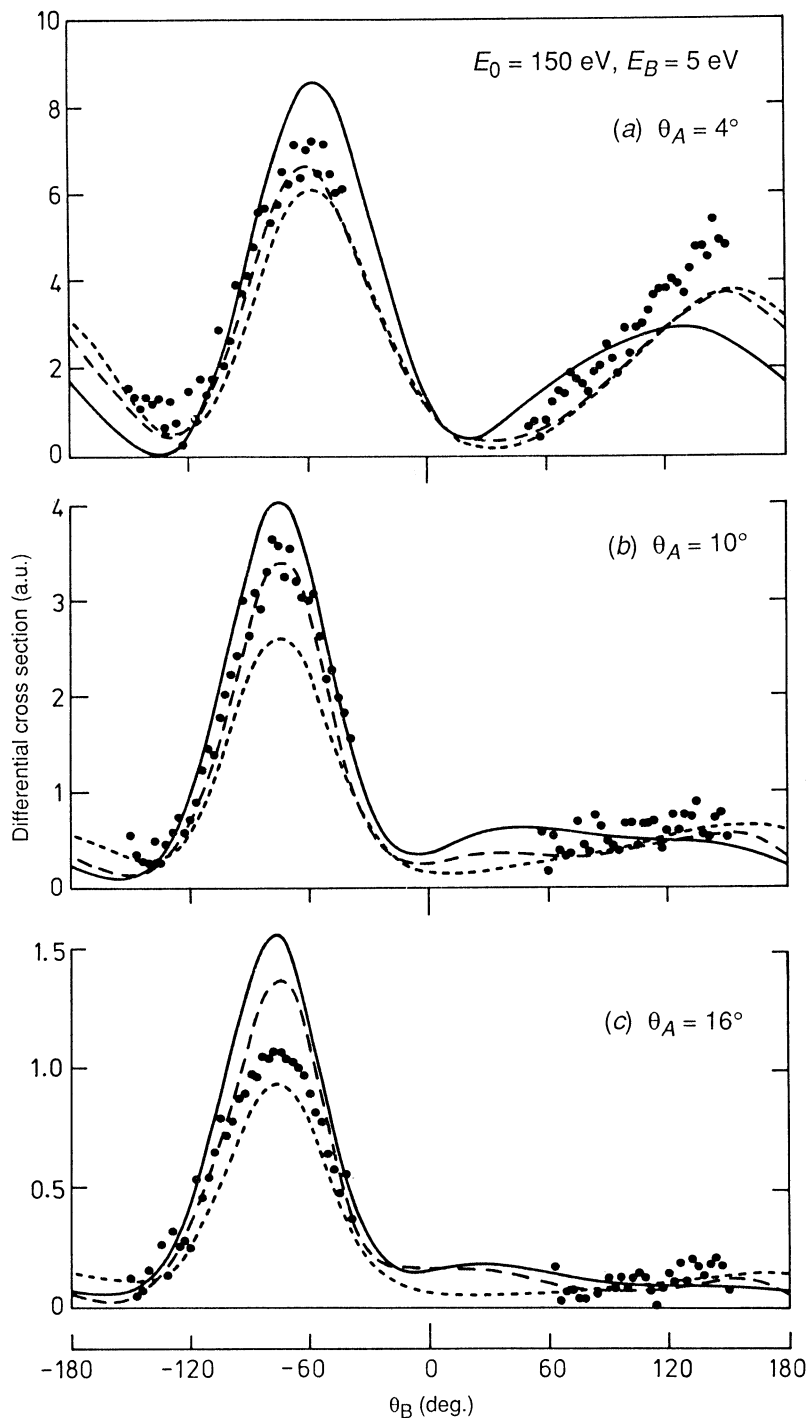


Fig. 9. Coplanar asymmetric differential cross section for the (e, 2e) reaction on hydrogen (Klar *et al.* 1987). Curves are full, DWBA; short-dashed, three-body approximation (Brauner *et al.* 1989); long-dashed, coupled pseudostate calculation with product final state (Curran and Walters 1987).

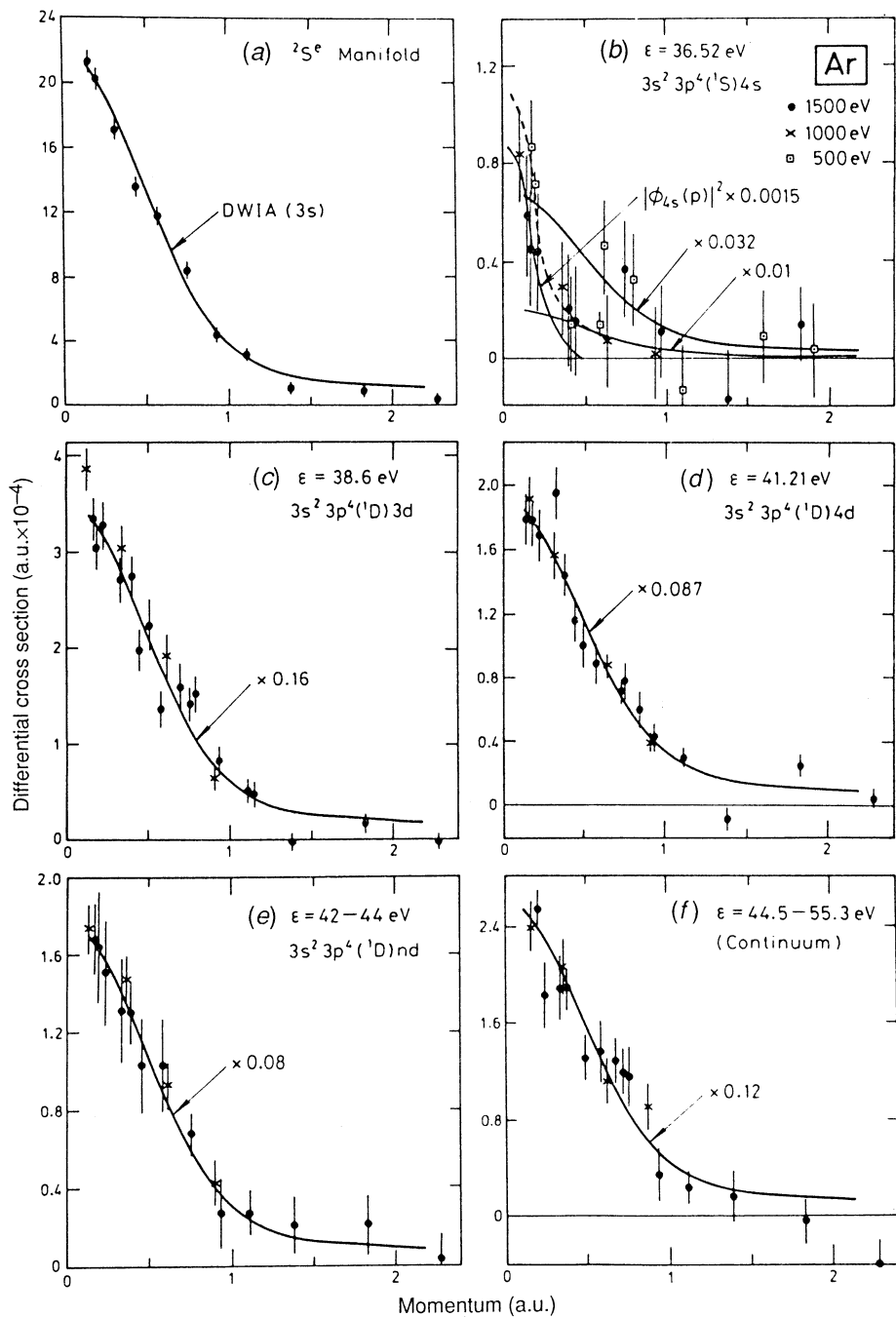


Fig. 10. The (e,2e) momentum distributions for the $2S^e$ manifold of argon. Curves are DWIA unless shown otherwise.

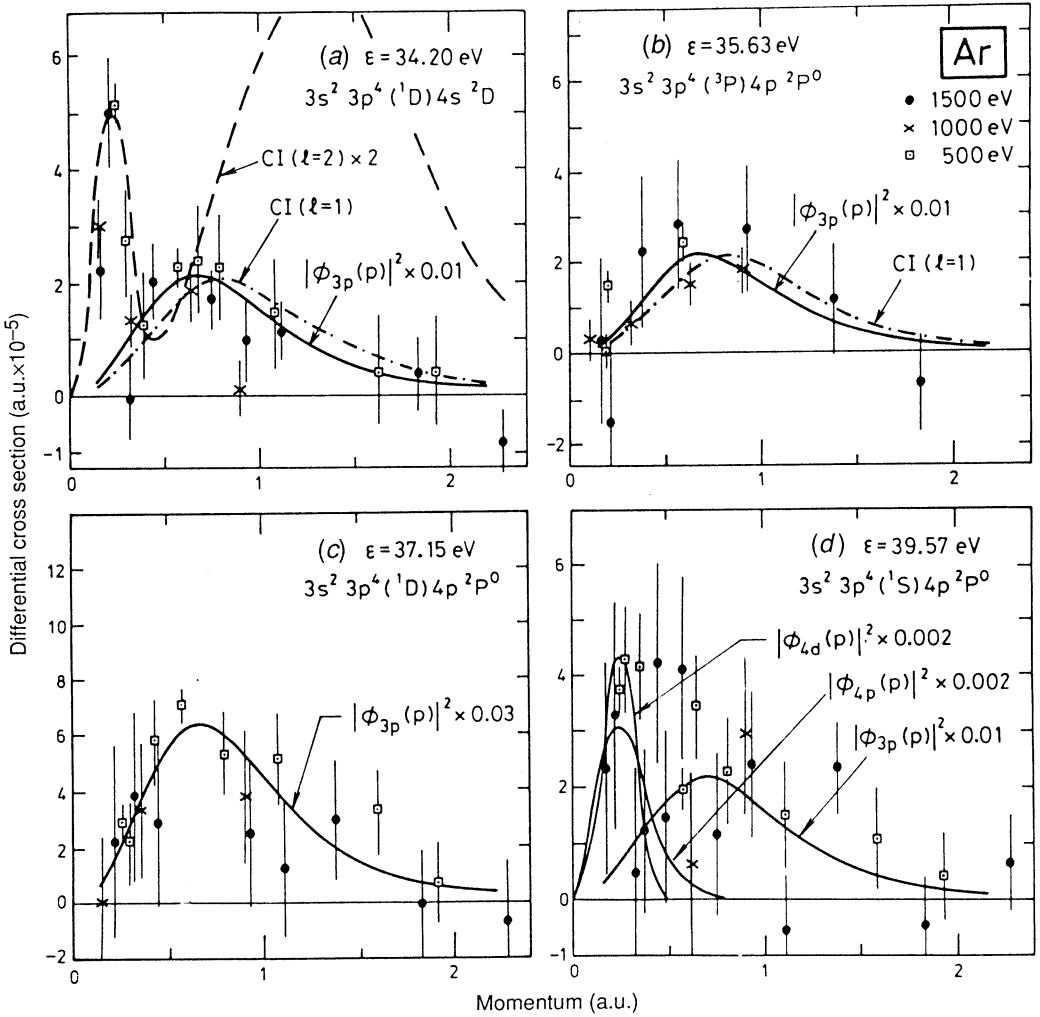


Fig. 11. The (e,2e) momentum profiles for the indicated states of Ar⁺. CI refers to the calculation of Mitroy *et al.* (1984).

5. Fine Details for Argon Structure

The type of structure detail available from (e,2e) is excellently illustrated by continuing our argon example. Figs 10 and 11 show the states above 34 eV observed in the 1500 eV noncoplanar symmetric experiment. Fig. 10a shows the 3s manifold (described here by the full notation ²S_e) described by the DWIA. Figs 10c to 10f clearly show states of the same manifold with their spectroscopic factors. Fig. 10b shows a state of the ²S_e manifold whose leading configuration is 3s² 3p⁴ (¹S) 4s. It is an ion state, like the 2s state in our helium example, which gives information about the 4s correlation in the target.

The state in Fig. 11a gives information about d correlations in the target. Figs 11b and 11c show correlations in the 3p ion manifold that can be described by the weak-coupling approximation, while the state of Fig. 11d again requires d correlations in the target.

Table 1. Spectroscopic factors for the 3s manifold of argon

Errors in the last figure are given in parentheses. References for columns are: Experiment (McCarthy *et al.* 1989), Overlap (Mitroy *et al.* 1984), Green's function (Amusia and Kheifets 1985)

Dominant configuration	Experiment		Overlap function	Green's
	ϵ_f (eV)	$ \langle i f\rangle ^2$		
3s 3p ⁶	29.24	0.55(1)	0.649	0.55
3p ⁴ 4s	36.50	0.02(1)	0.13	—
3p ⁴ 3d	38.58	0.16(1)	0.161	0.20
3p ⁴ 4d	41.21	0.08(1)	0.083	0.11
3p ⁴ 5s	42.65	0.08(1)	0.081	0.04
3p ⁴ 6d	43.40			
Ar ⁺⁺ +e		0.12(1)	0.013	

The spectroscopic factors $|\langle i|f\rangle|^2$ are the squares of the coefficients of the one-hole states in the eigenvectors for the states $|f\rangle$ resulting from the diagonalisation of the ion Hamiltonian in the weak-coupling representation. One such diagonalisation has been done by Mitroy *et al.* (1984). Table 1 compares the spectroscopic factors with the experimentally-determined ones and with the pole strengths resulting from a Green's function calculation by Amusia and Kheifets (1985).

We believe the experimental spectroscopic factors because the calculations from which they are extracted describe the whole experiment perfectly. In particular we note the comparison of the momentum distributions for the 3p and 3s manifolds (Fig. 6) and the momentum distributions of the individual states in the manifold (Fig. 10). Table 1 shows that quantum chemistry has some way to go in describing wave functions.

6. Molecules

The example of the argon atom has shown the kind of structure detail that can be extracted from the (e,2e) experiment. The same is true of the electronic states of molecules. The major difference is that we must use the PWIA for molecules because the non-central potentials make the distorted waves difficult to calculate.

Fortunately the PWIA works better for molecules than for atoms. Not only are momentum distribution shapes described very well up to $p \sim 2$ a.u. in 'normal' cases such as N₂ (Fig. 12) but the magnitudes of the momentum distributions for one-hole manifolds agree closely.

A very interesting 'abnormal' case is H₂O, where the states represented by the outermost orbitals have momentum distributions that do not agree with even completely-converged Hartree-Fock calculations in the PWIA. Our experience with the PWIA leads us to trust it and to blame the weak-coupling approximation. This is vindicated by Fig. 13 where curves 5 and 6 represent the converged Hartree-Fock calculations and curves 6c and 7c represent calculations of the target-ion overlap $\langle f|0\mathbf{p}\rangle$ performed with large CI expansions in each (Bawagan *et al.* 1987). Curves labelled by lower numbers are calculated with cruder orbitals. We conclude that the (e,2e) experiment reveals long-range correlations in the target.

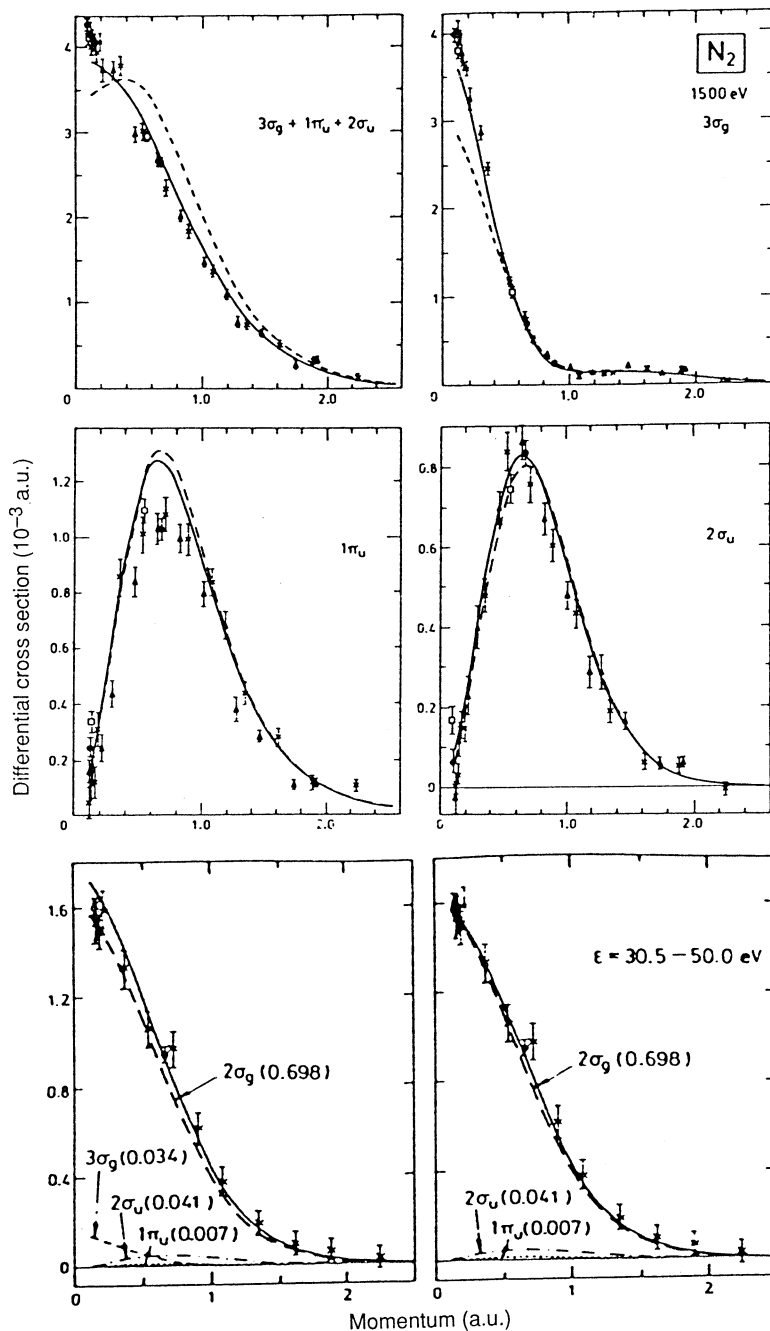


Fig. 12. The 1500 eV (e,2e) momentum distributions for nitrogen (Cook *et al.* 1990) compared with the PWIA. Solid curves use the spectroscopic factors from a Green's function structure calculation using SCF orbital wave functions in a $11s7p2d$ basis. Dashed curves for the outer-valence states use unit spectroscopic factors and a basis of double-zeta quality (Snyder and Basch 1972). The normalisation is preserved for the whole figure. Dashed curves for $\epsilon = 30.5 - 50.0$ eV represent the $11s7p2d$ orbitals which are added with the indicated spectroscopic factors to give the solid curve.

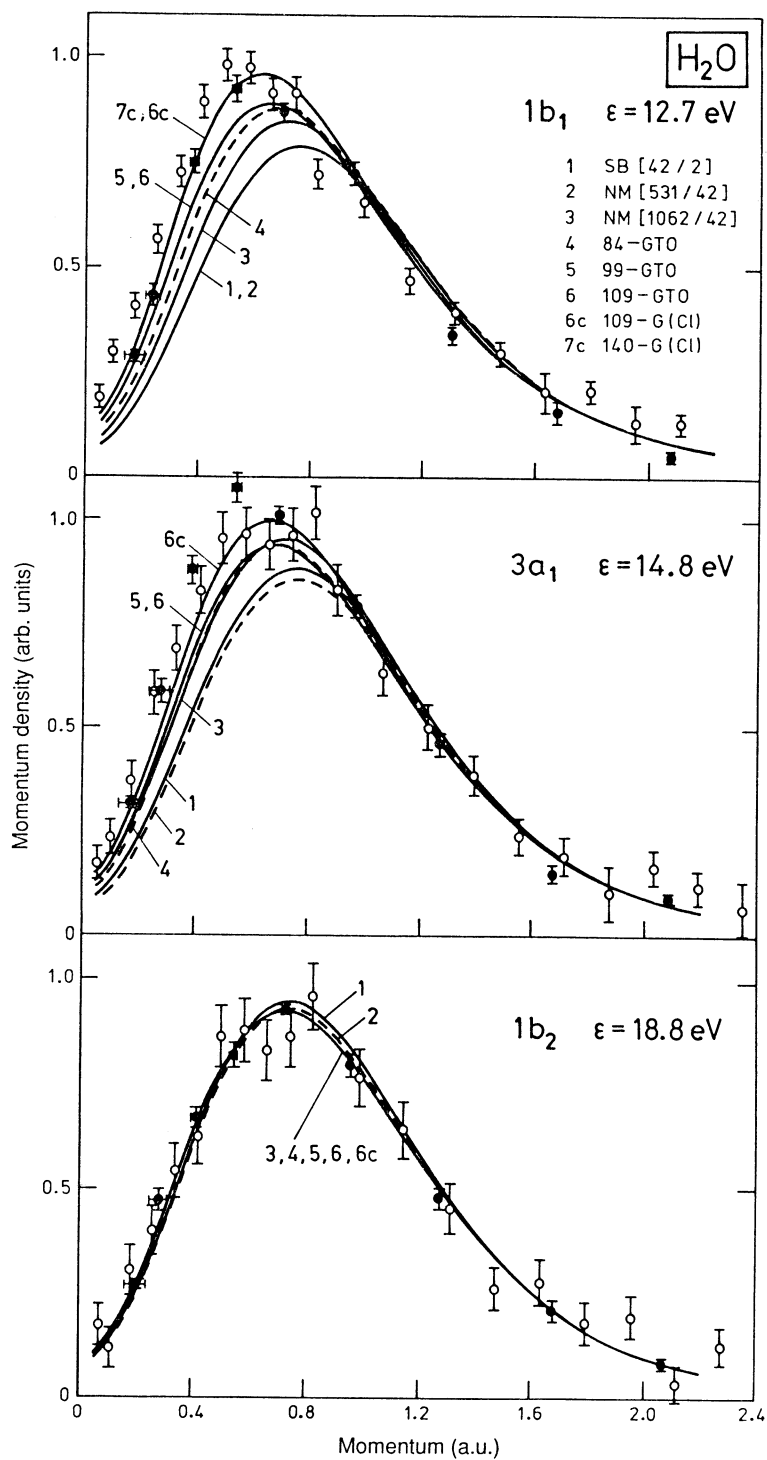


Fig. 13. The $(e, 2e)$ momentum distributions for the outer-valence orbitals of water (McCarthy and Weigold 1988). Curves are described in the text.

The situation with final-state (ion) correlations for molecules is very similar to that for atoms. The inner-valence manifolds are strongly split into states with quite large spectroscopic factors. The case of water, shown in Fig. 14, is typical. The solid curves here represent a simulated experimental energy distribution. In the weak-coupling approximation the cross sections for states at eigenvalues given by a structure calculation are given by the PWIA momentum distribution and the spectroscopic factor. These cross sections are spread by the experimental energy resolution (broken curves) and summed. The three lower-energy manifolds are not strongly split and are well described by the structure calculations. The theoretical spectroscopic factors for the inner-valence manifold are biased towards an energy that is too low.

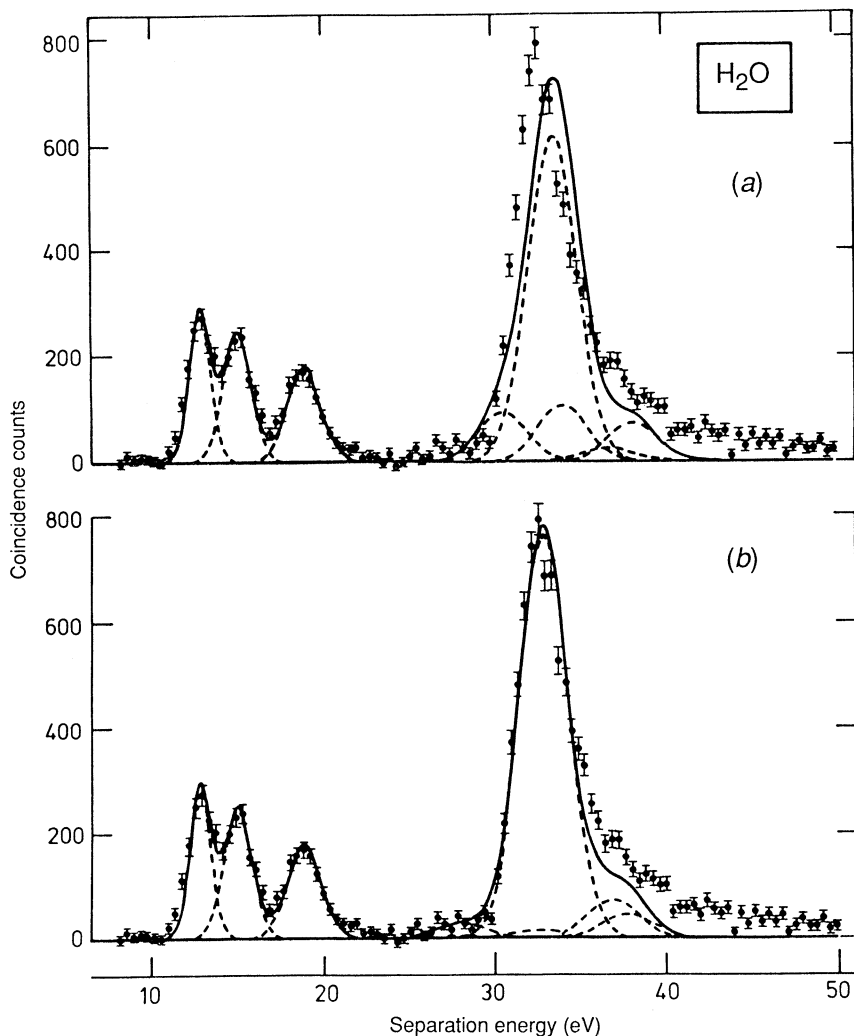


Fig. 14. Energy distribution for the valence states of water (McCarthy and Weigold 1988) at $E = 1000$ eV, $\phi = 0^\circ$. Curves are described in the text. The corresponding structure calculations are (a) Green's function (von Niessen *et al.* 1982) and (b) CI (Cambi *et al.* 1984).

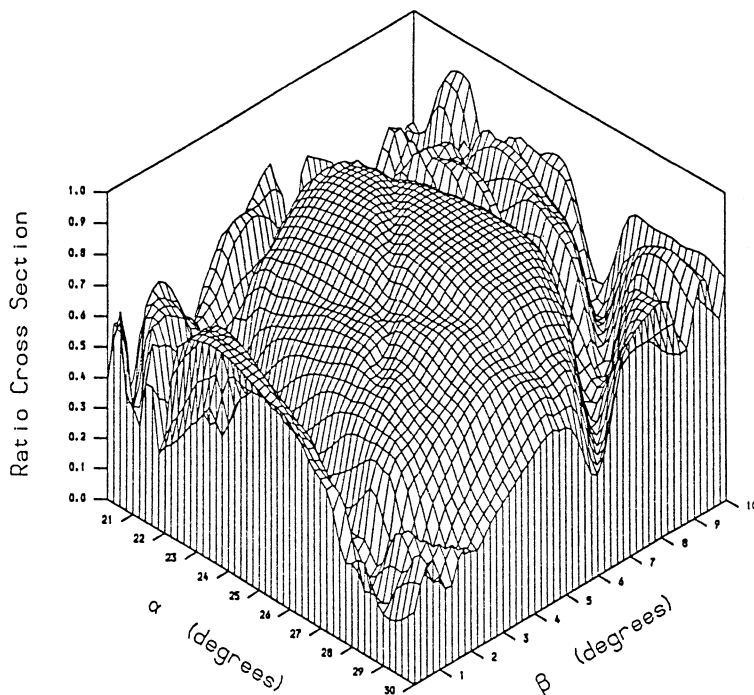


Fig. 15. Diffraction effects in the 30 keV (e,2e) reaction on a diamond crystal. Details are given in the text.

7. Solids

The understanding of solid-state (e,2e) experiments is just beginning (Ritter *et al.* 1984). They will be analysed using the DWBA, where the distorted waves are the wave functions of the dynamic diffraction theory of crystallography and the one-hole wave functions come from electron band theory (Allen *et al.* 1990, present issue p. 453). It may also be necessary to include a description of strongly-coupled plasmons in the details of the distorted waves.

For (e,2e) on a crystal it is important to find target orientations where Bragg diffraction does not invalidate the conclusion that the observed recoil momentum corresponds to the internal momentum of the electron. Fig. 15 shows the ratio of the differential cross section calculated without diffraction to that calculated (Matthews, personal communication 1989) with diffraction for a diamond crystal with a [1,1,1] surface normal and a thickness of 50 Å. The energies are $E = 30$ keV, $E_A = 28$ keV and the angles are chosen to include $p = 0$. The surface normal is initially in the incident electron direction and its orientation angles α, β are each swept through 10° . The plateaus on the diagram for a ratio of about 0.9 or more indicate the orientations for which diffraction does not significantly interfere with the measurement of the electron momentum distribution. These plateaus are large enough to suggest that the determination of band momentum distributions is feasible. The valleys in the diagram are due to a powerful diffraction plane being tracked through the Bragg condition.

Acknowledgment

This work was supported by the Australian Research Council.

References

- Allen, L. J., McCarthy, I. E., Maslen, V. W., and Rossouw, C. J. (1990). *Aust. J. Phys.* **43**, 453.
- Amusia, M. Ya., and Kheifets, A. S. (1985). *J. Phys. B* **18**, L679.
- Avaldi, L., McCarthy, I.E., and Stefani, G. (1989a). *J. Phys. B* **22**, 3305.
- Avaldi, L., Stefani, G., McCarthy, I. E., and Zhang, X. (1989b). *J. Phys. B* **22**, 3079.
- Bawagan, A. O., Brion, C. E., Davidson, E. R., and Feller, D. (1987). *Chem. Phys.* **113**, 19.
- Brauner, M., Briggs, J. S., and Klar, H. (1989). *J. Phys. B* **22**, 2265.
- Cambi, R., Ciullo, G., Sgamellotti, A., Brion, C. E., Cook, J. P. D., McCarthy, I. E., and Weigold, E. (1984). *Chem. Phys.* **91**, 373.
- Cook, J. P. D., Pascual, R., Weigold, E., von Niessen, W., and Tomasello, P. (1990). *Chem. Phys.* (in press).
- Curran, E. P., and Walters, H. R. J. (1987). *J. Phys. B* **20**, 337.
- Ford, W. F. (1964). *Phys. Rev. B* **133**, 1616.
- Klar, H., Roy, A. C., Schlemmer, P., Jung, K., and Ehrhardt, H. (1987). *J. Phys. B* **20**, 821.
- Lohmann, B., and Weigold, E. (1981). *Phys. Lett. A* **86**, 139.
- McCarthy, I. E., Pascual, R., Storer, P., and Weigold, E. (1989). *Phys. Rev. A* **40**, 3041.
- McCarthy, I. E., and Weigold, E. (1988). *Rep. Prog. Phys.* **51**, 299.
- Madison, D.H., McCarthy, I.E., and Zhang, X. (1989). *J. Phys. B* **22**, 2041.
- Mitroy, J., Amos, K. A., and Morrison, I. (1984). *J. Phys. B* **17**, 1659.
- Ritter, A. L., Dennison, J. R., and Jones, R. (1984). *Phys. Rev. Lett.* **53**, 2054.
- Snyder, L. C., and Basch, H. (1972). 'Molecular Wave Functions and Properties' (Wiley: New York).
- von Niessen, W., Cederbaum, L. S., Schirmer, J., Diercksen, G. H. F., and Kraemer, W. P. (1982). *J. Elec. Spectrosc.* **28**, 45.
- Weigold, E., Hood, S. T., and Teubner, P. J. O. (1973). *Phys. Rev. Lett.* **30**, 475.
- Weigold, E., and McCarthy, I. E. (1978). *Adv. At. Mol. Phys.* **14**, 127.

Manuscript received 1 March, accepted 3 May 1990

